The substrate effect in electron energy-loss spectroscopy of localized surface plasmons in gold and silver nanoparticles

Kadkhodazadeh, Shima; Christensen, Thomas; Beleggia, Marco; Mortensen, N. Asger; Wagner, Jakob Birkedal

Published in:
ACS Photonics

Link to article, DOI:
10.1021/acsphotonics.6b00489

Publication date:
2017

Document Version
Peer reviewed version

The substrate effect in electron energy-loss spectroscopy of localized surface plasmons in gold and silver nanoparticles

S. Kadkhodazadeh,[†,*] T. Christensen,[‡, §] M. Beleggia,[†,‖] N. A. Mortensen,[‡] and J. B. Wagner[†]

[†] *Center for Electron Nanoscopy, Technical University of Denmark, 2800 Kgs. Lyngby, Denmark*
[‡] *Department of Photonics Engineering, Technical University of Denmark, 2800 Kgs. Lyngby, Denmark*
[§] *Department of Physics, Massachusetts Institute of Technology, Cambridge, Massachusetts 02139, USA*
[‖] *Helmholtz-Zentrum Berlin für Materialen und Energie, 14109 Berlin, Germany*

ABSTRACT: Electron energy-loss spectroscopy (EELS) has become increasingly popular for detailed characterization of plasmonic nanostructures, owing to the unparalleled spatial resolution of this technique. The typical setup in EELS requires nanoparticles to be supported on thin substrates. However, as in optical measurements, the substrate material can modify the acquired signal. Here, we have investigated how the EELS signal recorded from supported silver and gold spheroidal nanoparticles at different electron beam impact parameter positions is affected by the choice of a dielectric substrate material and thickness. Consistent with previous optical studies, the presence of a dielectric substrate is found to redshift localized surface plasmons, increase their line-widths, and lead to increased prominence of higher order modes. The extent of these modifications heightens with increasing substrate permittivity and thickness. Specific to EELS, the results highlight the importance of the beam impact parameter and substrate related Čerenkov losses and charging. Our experimental results are compared with and corroborated by full-wave electromagnetic simulations based on the boundary element method. The results present a comprehensive study of substrate induced modifications in EELS and allow identification of optimal substrates relevant for EELS studies of plasmonic structures.

KEYWORDS: electron energy-loss spectroscopy, substrate, localized surface plasmons, silver, gold

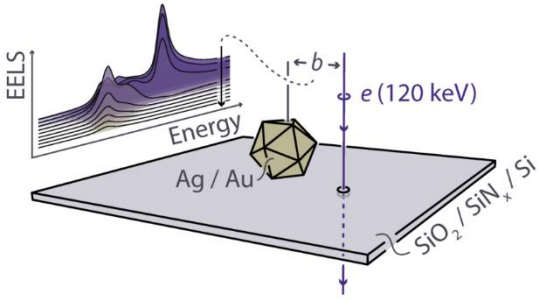

Noble metal nanoparticles have been studied extensively in the last few decades due to their remarkable optical properties, arising from the resonant interaction of their conduction electrons with incident light[1]. This phenomenon, known as localized surface plasmon (LSP) resonances, has enabled major developments in nanophotonics, with applications ranging from integrated optics and electronics[2] to solar cells[3] and biosensing[4]. The majority of these applications involve metallic nanoparticles and nanostructures supported on dielectric substrates. While several qualitative aspects of such setups can be appreciated and understood without an account of the neighboring dielectric environment[5,6], a complete account necessarily requires a full treatment of the entire optical environment, including the substrate. Partial accounts, which incorporate some features of the neighboring dielectric environment, for instance through effective homogeneous cladding approximations[7,8], have been shown to improve quantitative agreement between measurements and theory. However, they omit several important characteristics of the compound system, whose properties require a fuller description[9–13]. Several of those features can be treated within the image dipole perspective; there, the induced polarization of the nanoparticle introduces an induced polarization in the substrate, taking the form of a sum of multipoles at the image position. This multiple scattering coupling between the nanoparticle and its images may significantly modify several key optical features of unsupported nanoparticles, exemplified by highly non-uniform field distributions in the nanoparticle-substrate vicinity, spectral shifts, and increased coupling to higher-order (HO) multipoles[13,14].

Several previous studies have experimentally explored the substrate effect in the context of ensemble-averaged optical measurements on nanoparticle arrays fabricated by electron beam lithography[15–17], demonstrating a clear dependence of the LSP energy on substrate dielectric properties. However, averaging and convoluting the influence of the substrate with, for example, nanoparticle size or shape variation, cannot be avoided in ensemble studies. Correlative probing of the optical response and structural properties at single particle level, using optical and *ex-situ* transmission electron microscopes (TEMs) studies, has been carried out for gold (Au) and silver (Ag) nanocubes, where both the dielectric properties and the thickness of a substrate were found to have a large effect on optical properties[18,19]. A powerful technique for the characterization of plasmonic properties is EELS performed in a TEM, which enables *in-situ* correlative studies of optical and structural properties[20,21]. Improvements made in the energy resolution in TEM to below 0.2 eV in the last two decades has made the optical energy range in EELS

accessible, allowing LSPs to be probed and studied with sub-nanometer spatial resolution[6,8,22–26]. TEM requires specimens thin enough to be electron transparent (typically below 100 nm) and therefore, plasmonic nanoparticles studied by EELS are typically supported on thin membranes[6,8,27] or buried in a thin embedding material[28]. In many cases, modest attention has been given to the influence of the substrate, where it is either not taken into account[6,8,29] or assumed to act as a homogeneous background medium, whose effective permittivity is fitted by comparing simulations to experimental results[27,30,31]. More recently, a number of studies have focused on specific substrate induced effects in EELS, such as mode splitting and energy transfer between LSPs and the substrate in the optical response of truncated nanospheres and nanocubes[32–35]. In this work, we investigate the substrate effect in EELS through a systematic study of the LSP resonances appearing in the EELS spectra of Ag and Au nanoparticles supported on a variety of substrates, allowing a full examination of the role of substrate material composition and thickness. Furthermore, motivated by our recent findings of strong dependence of the EELS signal on the position of the electron beam relative to the particle (impact parameter)[28], we additionally investigate this dependence and its interplay with substrate parameters. Throughout, the experimental findings are compared with accurate and fully retarded simulations of the EELS signal computed using the boundary element method.

RESULTS

AG NANOPARTICLES. STEM images of the Ag and Au nanoparticles and a schematic illustration of the relative geometric parameters are presented in Figure 1. The examined nanoparticles were found to have close to spherical geometries with diameters $2R = 20.4 \pm 1.5$ nm in the case of Ag, and $2R = 53.5 \pm 2.3$ nm in the case of Au (averaged measurements from 30 nanoparticles in each case). The particle diameters fall outside the range of significant non-classical corrections, *e.g.* due to nonlocality[36], thus justifying the local response treatment of the EELS signal. Larger Au particles were deliberately chosen to ensure satisfactory levels of signal in the experimental EELS data, as EELS data collected from Au particles generally contain low signal to noise ratios.

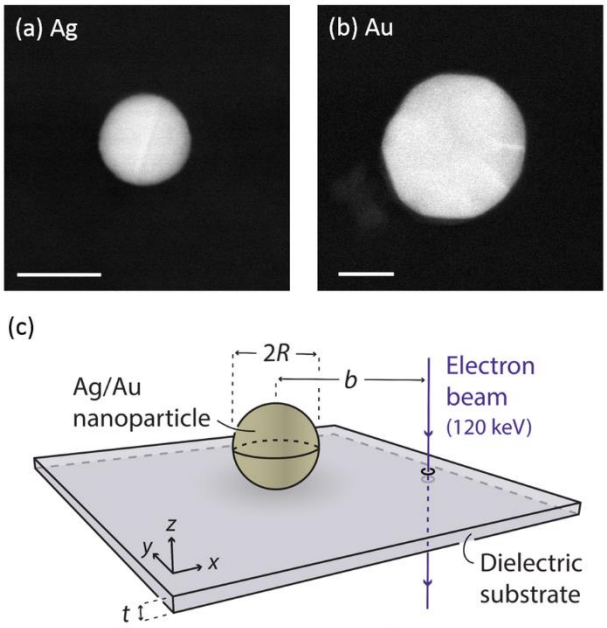

Figure 1: High-angle annular dark-field STEM images of (a) Ag and (b) Au nanoparticles. The length of the scale bar in each case is 20 nm. (c) A schematic illustration of the considered setup, highlighting the relevant parameters in the experiments.

The simulated EEL spectra calculated for a $2R$ = 20 nm Ag nanosphere in vacuum and embedded in infinitely thick SiO_2, SiN_x and Si media as functions of the beam impact parameter b are summarized in Figure 2. While these setups are unrealizable experimentally, they provide a useful point of reference for comparison with the substrate-supported particles. In the case of Ag particle in vacuum (Figure 2 (a, e)), three distinct regions within the examined impact parameter range are identified:

Region (i): $1.5R$ (15 nm) < b < $2R$ (20 nm): a single peak at ~ 3.5 eV, corresponding to the dipole excitation, is observed.

Region (ii): $1R$ (10 nm) < b < $1.5R$ (15 nm): in this region additional peaks, corresponding to the excitation of HO modes, appear and intensify with decreasing b. It is important to stress here that while distinct HO modes can clearly be distinguished in the unbroadened simulated data, we will in general not have sufficient energy resolution to resolve individual multipole peaks experimentally[28]. Instead, a single broad peak will be observed in the EEL spectrum; this is reproduced by the broadened simulated data, which accounts qualitatively for this finite energy resolution.

Region (iii): $b < R$ (10 nm): in this region a final additional peak emerges at ~ 3.8 eV, corresponding to the excitation of the bulk plasmon. In contrast to regions (i) and (ii), HO modes have magnitudes comparable to or higher than the dipole LSP mode in this region.

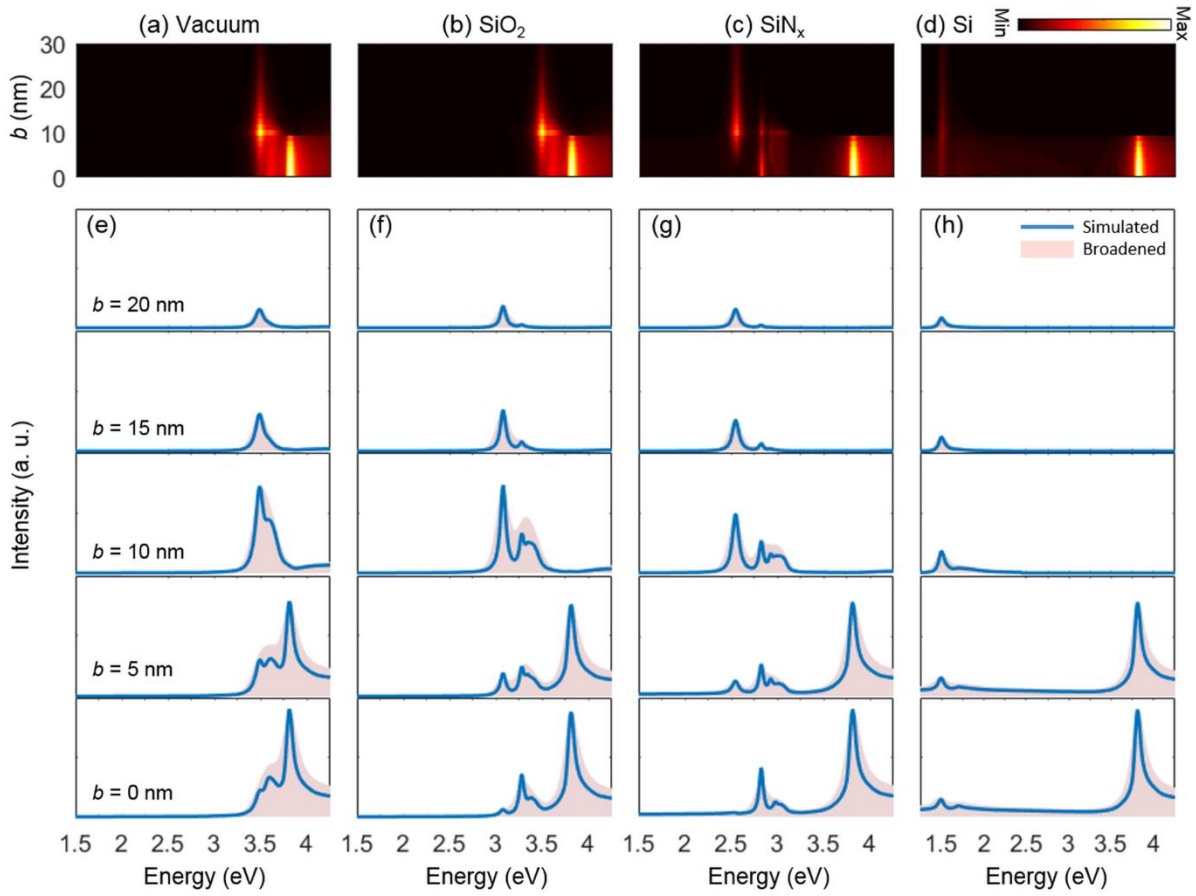

Figure 2: Simulated EELS intensity maps and spectra at selected impact parameter positions simulated for a $2R$ = 20 nm Ag nanosphere fully embedded in (a, e) vacuum, (b, f) SiO_2, (c, g) SiN_x, and (d, h) Si. Pink filled areas in (e – h) denote the simulated spectra convoluted with a Gaussian envelope with FWHM of 0.15 eV, accounting for the energy resolution of the experiments.

Overall, the same trend can be identified in the EELS response of the embedded particles, with the dipole LSP being largely the dominant feature in region (i), HO LSPs intensifying in region (ii) and the bulk plasmon, as well as the dipole and HO LSPs being present in region (iii). However, two major distinctions in the plasmonic response of the embedded Ag particles relative to that of the Ag particle in vacuum can be observed: one is the redshift of the LSPs, increasing from SiO_2 to Si (the center energy of the dipole LSP occurring at ~ 3.1 eV, ~ 2.5 eV and ~ 1.5

eV for particles embedded in SiO_2, SiN_x and Si, respectively), and the other is the higher number of HO modes discernable in the spectra at given *b* positions.

The following observations are made when examining the simulated EELS spectra of Ag nanoparticles supported on SiO_2 substrates with thicknesses t = 8 nm and 20 nm, presented in Figure 3: In region (i) ($b > 1.5\ R$) the dipole LSP mode is the main feature in the EEL spectra, although a weak shoulder due to HO modes can also be discerned in Figure 3d. Only a slight redshift of the dipole LSP with respect to its frequency in vacuum (~ 0.05 eV) is observed here compared to the embedded scenario. Broadening the simulations with a Gaussian function increases the line-width of the plasmon feature but the center energy of this feature remains unchanged, since the probability of exciting HO modes within this impact parameter range remains low. This indicates that the main plasmon feature in the EEL spectra acquired in this region can be directly interpreted as the dipole LSP mode. In region (ii) ($R < b < 1.5\ R$) the spectral features associated with HO modes become increasingly prominent, with the onset of significant modifications to the dipole-only response occurring at comparatively larger *b* than that for an unsupported particle. Broadening the simulated data here smears out the dipole and HO modes and produces a single broad peak encompassing all LSP excitations. As the result, the LSP feature in the broadened data is blueshifted relative to the dipole mode, due to the increasing intensity of the HO modes. In region (iii) ($b < R$) the bulk plasmon, as well as the dipole and HO modes are present. The HO modes in this region have intensities comparable to that of the dipole mode. Subsequently, the single LSP feature in the broadened spectra is further blueshifted relative to the dipole LSP mode.

Comparing the spectra in Figures 3(e) and (f) shows that broadening the simulated data reproduces many of the features observed experimentally. In particular, there is good agreement between the energies at which different spectral features occur. However, all excitations still have wider line-widths in the experimental data and the bulk plasmon intensity is consistently overestimated in the simulations. The overestimation of the bulk plasmon intensity in similar simulations has been observed by others[29,37,38] and has been ascribed to further attenuation of the beam inside the metallic nanoparticles in experiments, not accounted for in the simulations[37]. Moreover, the simulations assume a normal incident angle of electrons relative to the substrate and negligibly small post specimen scattering collection angles, while the experiments employ a convergent electron probe with convergence semi-angle of ~ 25

mrad and a collection semi-angle of ~ 28 mrad. The plasmon energy is a function of the scattering vector and shifts to larger values at higher scattering angles[39]. The relatively large acceptance angle of the EELS spectrometer here allows collection of a range of scattering angles, resulting in a slight blueshift and broadening of the recorded plasmon features. Additional damping of the plasmon excitations through transfer of energy to single electron transitions, given the relatively large scattering collection angle in the experiments is also possible[40]. Other possible contributing factors to the observed increased line-widths of the plasmon features include Kreibig damping[41,42] and structural defects[43,44] and impurities present in the Ag nanoparticles.

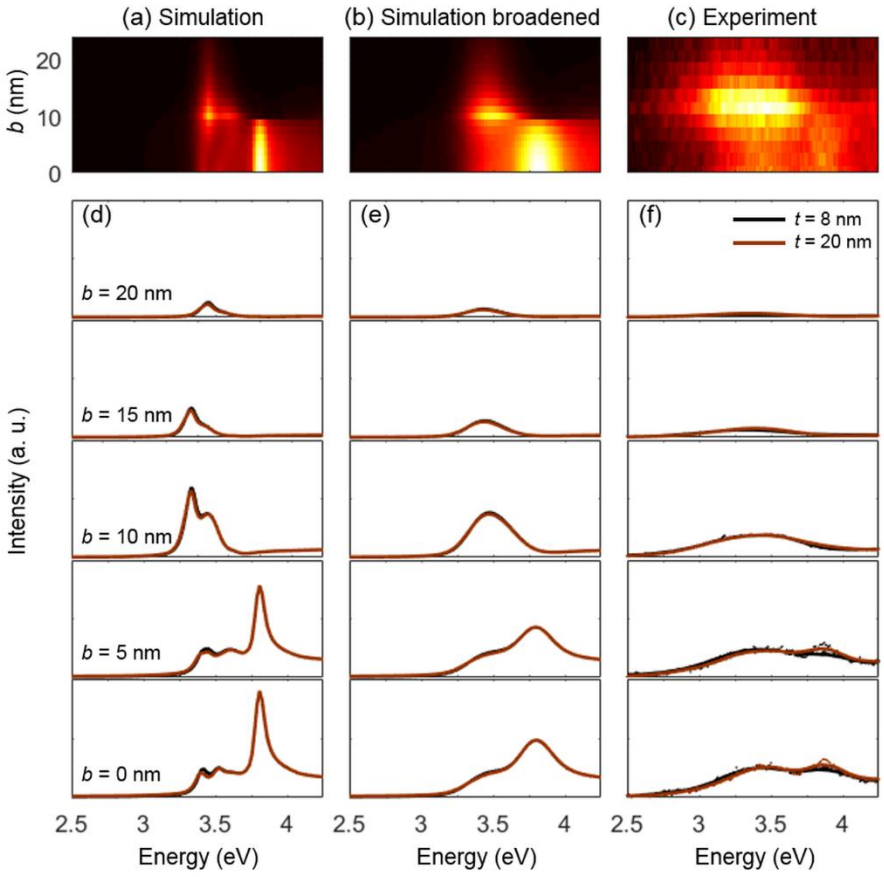

Figure 3: EELS intensity maps and selected spectra at different impact parameter positions simulated for a $2R$ = 20 nm Ag nanoparticle (a, b, d, e) and experimentally acquired from $2R$ ~ 20 nm Ag nanoparticles (c, f) supported on t = 8 nm and 20 nm SiO_2 substrates.

Overall, only minor differences are observed between the EEL spectra of particles on t = 8 nm and 20 nm SiO_2: in both experimental and simulated spectra, the relative intensity of HO to dipole modes is slightly increased for the thicker substrate, and a slightly larger redshift of the LSP modes for the thicker substrate is found in the simulations.

The experimental and simulated EEL spectra for Ag nanoparticles supported on t = 5 nm and 20 nm SiN_x substrates are shown in Figure 4. The simulated results show significant changes in the EEL spectra of the Ag nanoparticle compared to those in vacuum and SiN_x media and on a SiO_2 substrate: while previously only one dominant feature was present in region (i), in the case of the Ag nanoparticle on SiN_x, at least 3 different features with similar intensities are present. The energies at which the dipole and HO modes occur are redshifted compared to both particles in vacuum and on a SiO_2 substrate (the dipole mode shifted by ~ 0.2 eV for Ag supported on a t = 5 nm substrate relative to Ag in vacuum). Increasing substrate thickness results in larger levels of background signal, increasing redshift of the LSP modes and increasing relative intensity of HO to dipole modes. The separate dipole and HO modes present in the simulated spectra disappear after applying Gaussian broadening (due to comparable intensities of the dipole and HO LSPs in this region) and are replaced with a broad feature, whose center energy does not correspond to that of the dipole LSP. This implies that the LSP feature recorded experimentally from Ag nanoparticles on SiN_x substrates in region (i) can no longer be interpreted as having mainly dipolar characteristics. Obtaining EEL spectra containing primarily the contribution from the dipolar LSP consequently requires acquisition at even larger impact parameters. However, acquiring EEL spectra with adequate signal to noise ratios at $b > 2\ R$ can prove to be a challenge. In region (ii), the intensity of the HO modes continues to increase and exceeds that of the dipole mode. Accordingly, the center energy of the broadened LSP feature in this region continually blueshifts with decreasing b. Region (iii) in the experimental data is again marked by the appearance of the bulk plasmon. The same discrepancy between the intensity of the bulk in the simulated and experimental spectra exists here as did in the case of Ag particles on SiO_2 substrates.

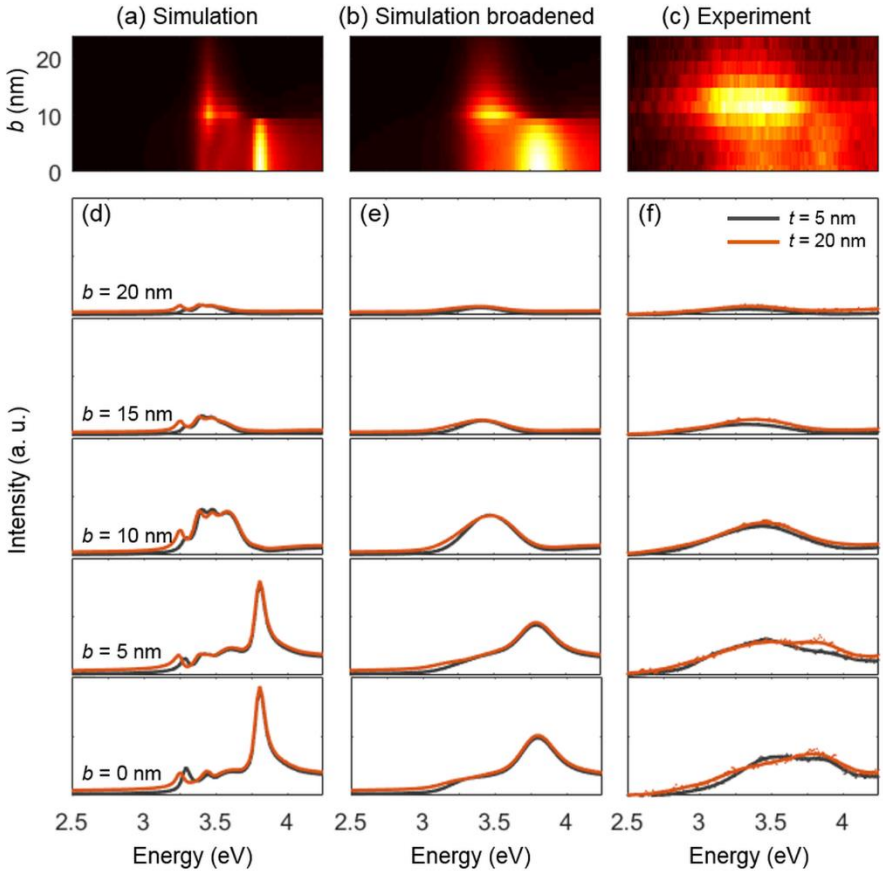

Figure 4: EELS intensity maps and selected spectra at different impact parameter positions (a, b, d, e) simulated for a $2R$ = 20 nm Ag nanoparticle (a, b, d, e) and experimentally acquired from $2R$ ~ 20 nm Ag nanoparticles (c, f) supported on t = 5 nm and 20 nm SiN_x substrates.

The most considerable modification in the plasmonic response of the Ag nanoparticles is seen in the case of particles on a Si substrate, as the EEL spectra in Figure 5 do not resemble those of nanoparticles in vacuum or embedded in Si: all spectral features in the simulated data are much broader and are strongly redshifted compared to those calculated for particles in vacuum, on SiO_2 or SiN_x substrates. Two prominent spectral features can be seen in region (i): the dipole LSP mode at ~ 2.9 eV and a HO LSP mode at ~ 3.5 eV. The relative intensity of the HO to dipole modes increases with decreasing b and similar to what was observed for SiN_x, the intensity of the HO LSPs already exceeds that of the dipole LSP in this region. This trend continues throughout the studied impact parameter range. No additional features appear in region (ii). The bulk plasmon feature is present at ~ 3.8 eV in region (iii), as expected. Contrary to what was observed for SiO_2 and SiN_x substrates, broadening the simulated data here makes little difference to the overall appearance of the EEL spectra, since all the features present are already quite broad. Increasing t produces the same effect on the center energy, relative intensity of the dipole to HO modes and the

background signal, as discussed previously. A practical implication of the broad line-widths of the features and the large background signal from the substrate is reduced signal to noise ratio and poor visibility of spectral features, making analyzing the experimental data particularly challenging. This is evident in the experimental results in Figure 5, where the HO mode at 3.5 eV and the bulk plasmon at 3.8 eV are difficult to resolve.

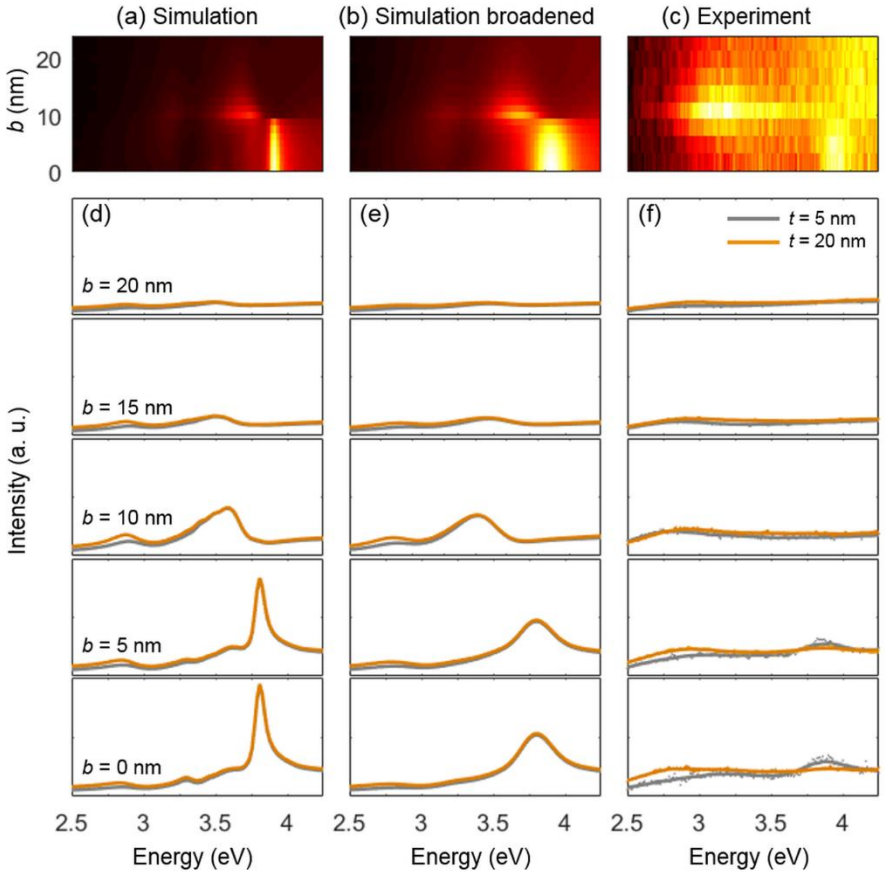

Figure 5: EELS intensity maps and selected spectra at different impact parameter positions (a, b, d, e) simulated for a $2R$ = 20 nm Ag nanoparticle (a, b, d, e) and experimentally acquired from $2R$ ~ 20 nm Ag nanoparticles (c, f) supported on t = 5 nm and 15 nm Si substrates.

AU NANOPARTICLES. Simulated intensity images and selected EELS spectra computed for $2R$ = 50 nm Au nanoparticles in vacuum and embedded in SiO_2, SiN_x and Si media are presented in Figure 6. In the case of an Au particle in vacuum, little difference is found between regions (i) ($1.5R < b < 2R$) and (ii) ($R < b < 1.5\ R$), where all spectra contain a single broad peak at ~ 2.4 eV. In region (iii) ($b < R$), still only a single broad peak is present in the spectra but at a slightly higher energy of ~ 2.5 eV. Since here the electron beam transverses the particle and that the bulk plasmon in Au occurs at 2.5 eV[25,45], this observed energy shift signifies the predominantly bulk

plasmon nature of this peak in region (iii). The simulated EELS response of an Au nanoparticle embedded in SiO_2 features the dipole LSP at ~ 2.3 eV in regions (i) and (ii) and the bulk plasmon at ~ 2.5 eV in region (iii). The dipole LSP of Au nanoparticles embedded in SiN_x and Si are additionally redshifted compared to particles in vacuum (occurring at ~ 2.0 eV and ~ 1.25 eV, respectively). Moreover, similar to the EELS response of Ag particles in Figure 2, HO LSP modes are also present in the spectra simulated for Au particles embedded in SiN_x and Si, and increase in magnitude with decreasing *b*.

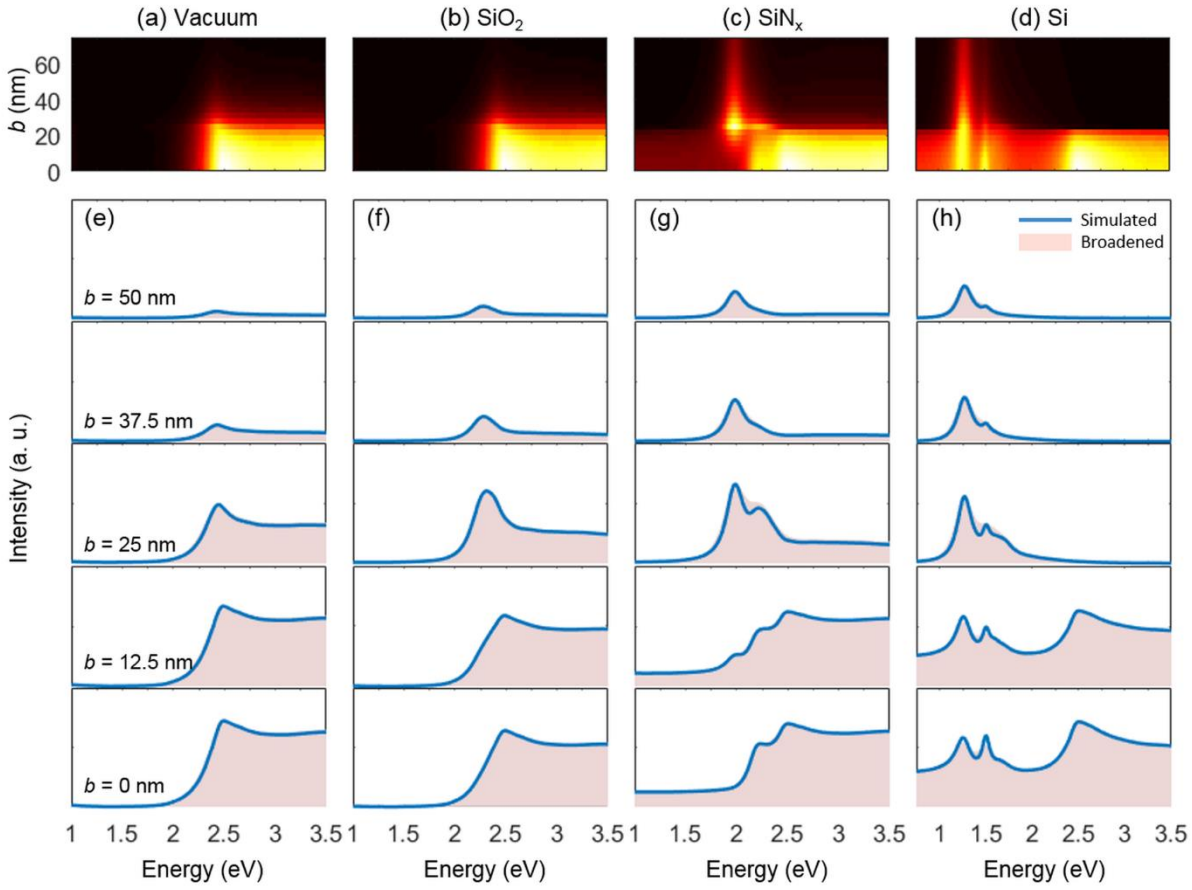

Figure 6: Simulated EELS intensity maps and spectra at selected impact parameter positions simulated for a $2R$ = 50 nm Au nanoparticle fully embedded in (a, e) vacuum, (b, f) SiO_2, (c, g) SiN_x, and (d, h) Si. Pink filled areas in (e – h) denote the simulated spectra convoluted with a Gaussian envelope with FWHM of 0.15 eV.

Figure 7 summarizes the simulated and experimental results acquired for Au nanoparticles supported on various substrate materials and thicknesses. Overall, little difference is detected between the simulated EEL spectra of supported Au particles and in vacuum: regions (i) and (ii) feature only the dipole LSP (redshifted by 0.04 eV for Au particle supported on 5 nm thick Si substrate relative to the dipole LSP of particle in vacuum) and region (iii)

contains predominantly the bulk plasmon. The same pattern is observed in the experimental data, with the LSP at ~ 2.4 eV present in regions (i) and (ii) and the bulk plasmon in region (iii). Throughout, much poorer signal to noise ratio is detected from Au particles compared to Ag, as it is clear from the spectra in Figure 7(f).

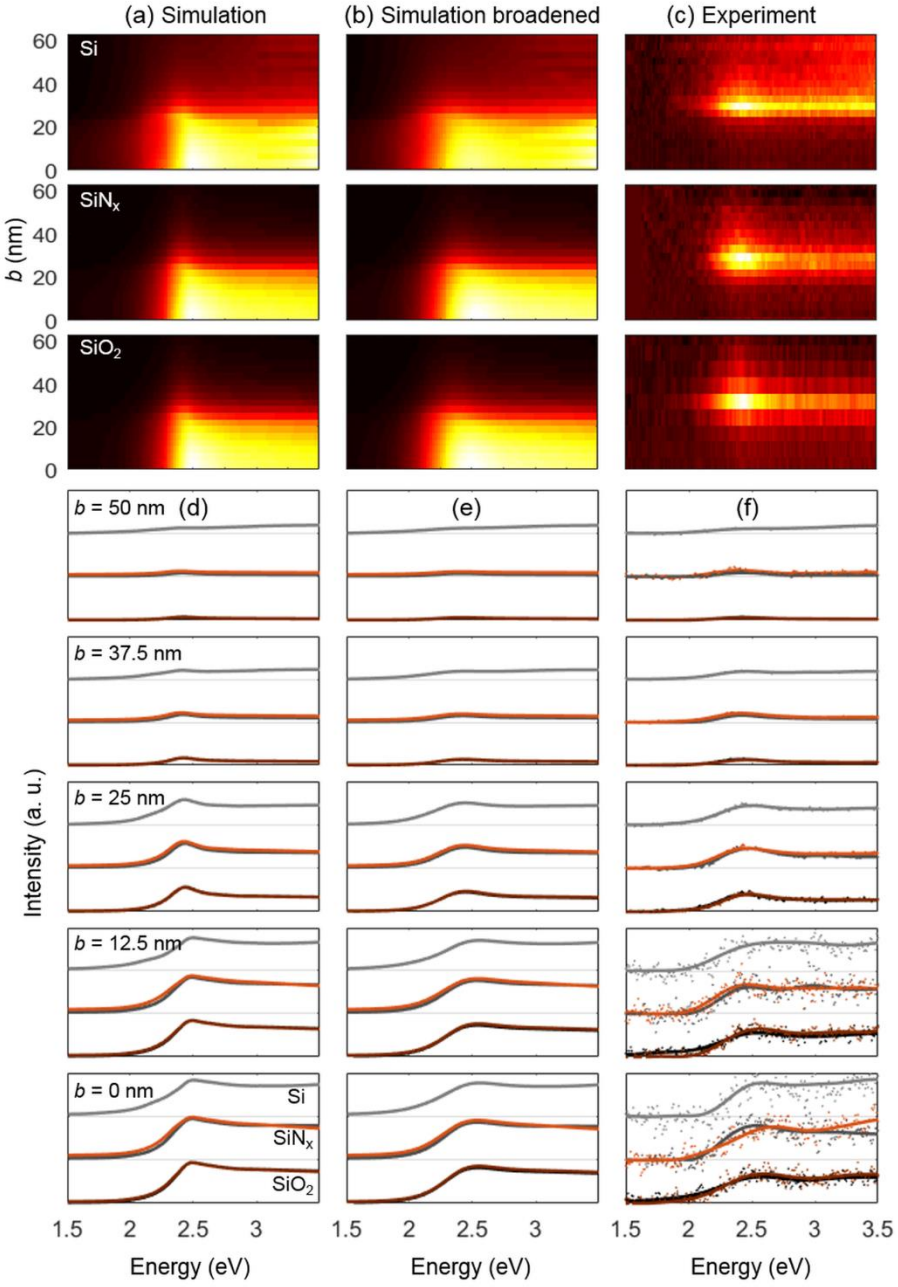

Figure 7: EELS intensity maps and selected spectra at different impact parameter positions simulated for a $2R$ = 50 nm Au nanoparticle (a, b, d, e) and experimentally acquired from $2R$ ~ 50 nm Au nanoparticles (c, f) supported on SiO_2, SiN_x and Si substrates. The spectra in (d – f) follow the same color presentation as in Figures 3 – 5 (SiO_2: t = 8 nm in black and t = 20 nm in brown; SiN_x: t = 5 nm in dark gray and t = 20 nm in red; Si: t = 5 nm in light gray).

DISCUSSIONS

The results presented demonstrate that the substrate can significantly affect the EELS measurements of LSPs. For a dielectric substrate, the modifications induced include redshift in the resonance energy of LSPs, increased probability of exciting higher order modes and increased damping of the LSPs. Here, we explore how different parameters influence the extent of these modifications.

SUBSTRATE MATERIAL. Of the three substrate materials studied, SiO_2 and SiN_x are insulators and are expected to be effectively lossless in the energy range considered. For non-insulating substrate materials, contributions in EEL spectra due to substrate losses are anticipated. Si, for instance, is a semiconductor with a bandgap of ~ 1.4 eV and subsequently, loss features due to the substrate itself can be present above the bandgap. Moreover, due to the close proximity of the nanoparticles and the substrate, LSPs are afforded an additional decay channel via the lossy substrate, which leads to increased plasmon line-width[35], as observed here. Additionally, the substrate induced redshift in the LSP energy and the probability of exciting HO modes exhibit dependence on substrate material. The influence of the substrate on the properties of the dipole LSP can be assessed qualitatively by considering the semi-infinite substrate in an image-dipole approximation: the dipole resonance condition for a spherical nanoparticle with permittivity ε, supported on an infinitely thick substrate with permittivity ε_{sub} and embedded in a medium with permittivity ε_{med} can be described by a quasistatic resonance condition within the image-dipole approximation[46–48]:

$$\varepsilon_{\mathrm{med}} + L_{\parallel,\perp}(\varepsilon - \varepsilon_{\mathrm{med}}) = 0 \qquad (1)$$

with so-called depolarization factors[49] defined by: $L_{\parallel,\perp} = {}^{1}\!/_{3}\left\{1 - \frac{\eta_{\parallel,\perp}}{8}\frac{\varepsilon_{\mathrm{sub}}-\varepsilon_{\mathrm{med}}}{(\varepsilon_{\mathrm{sub}}+\varepsilon_{\mathrm{med}})}\right\}$. Here, $\eta_{\parallel,\perp}$ expresses the fact that the substrate splits the three-fold dipole-degeneracy into two partitions based on the orientation of the LSP dipole moment (in-plane $\eta_{\parallel} = 1$ and out-of-plane $\eta_{\perp} = 2$). The influence of the substrate, relative to its absence, is thus to redshift the dipole LSP: *e.g.*, for a pure Drude metal ($\varepsilon = 1 - \omega_{\mathrm{p}}^2/\omega^2$) in a vacuum embedding ($\varepsilon_{\mathrm{med}} = 1$), the resonance frequency is shifted from $\omega_{\mathrm{p}}/\sqrt{3}$ to $\omega_{\mathrm{p}}\sqrt{L_{\parallel,\perp}}$, i.e. to the red since $L_{\parallel,\perp} < 1/3$ for $\varepsilon_{\mathrm{sub}} > 1$. The splitting between in- and out-of-plane oriented dipole LSPs, is too small to observe in the present experiments, contributing instead as additional broadening to the main dipole peak. Overall, the depolarization factors $L_{\parallel,\perp}$ decrease monotonically with increasing $\varepsilon_{\mathrm{sub}}$, forcing the redshift to similarly increase with the substrate

permittivity: the same trend is observed in our experimental results (see Figures S1 and S2 in the Supporting Information (SI)). Moreover, the probability of exciting HO LSPs increases with increasing $\varepsilon_{\mathrm{sub}}$, since the local contrast in dielectric environment acts to break the translational symmetry of the embedding material, thereby providing an additional source of momentum through secondary scattering of the incident field of the electron probe[9,50].

A further consideration for choosing a substrate is its tendency to charge when exposed to an electron beam, due to, for example, secondary electron emission from the irradiated area. For metals or good conductors, any net local charge is neutralized on a time scale that is much smaller than the dwell-time of the beam at a particular position during image acquisition. For poor conductors, the dielectric relaxation time, $\tau_{\mathrm{d}} = \rho\varepsilon_{\mathrm{sub}}$, where ρ is the nominal film resistivity, may become comparable to the beam dwell-time, resulting in injection of charges (which can be mobile or non-mobile depending on the specific inelastic processes involved) in the illuminated area of the substrate. In extreme cases, substrate charging can inhibit data acquisition by causing the electron beam to be deflected[51] and therefore, wide bandgap substrate materials are in general not favorable when charging is concerned. When employing insulating substrates, it could be necessary to reduce the electron beam current or beam dwell time per image pixel in order to mitigate the practical implications of charging. In our case, some levels of image drift and specimen instability were experienced during data acquisition from particles supported on SiO_2 and SiN_x substrates, but only when higher acquisition times or beam currents were used. Besides these practical implications, charging can also modify the EELS signal: if injected charges are mobile and confined to the surface of the substrate, their role can qualitatively be described as a change in the (quasistatic) reflection coefficient, which contributes to the polarizability tensor. In cases where τ_{d} is comparable to the acquisition time at each point along a line-scan, the electron beam will effectively be dragging a localized charge spot along and would require the treatment of the particle interacting with an external point charge. In all cases, a systematic study of beam-induced charge dynamics is necessary to properly comprehend the consequences of charging in EELS. Here, while substrate charging was not found to interfere with data acquisitions, we cannot exclude the role of substrate charging in the observed discrepancies between theory and simulations, in particular the excessive broadening and the differences in the observed probabilities.

SUBSTRATE THICKNESS. The assumption of a semi-infinite substrate underlying Eq. (1) necessarily entails an overestimation of the substrate-induced redshift and also neglects the thickness-dependence of the substrate. The treatment can be generalized, however, by introducing an additional image dipole to account for the finite substrate thickness, *t*. Doing so (for weakly reflective substrates with $t/R \gg 1$), the depolarization factors generalize to $L_{\parallel,\perp}(t) \simeq \frac{1}{3}\left\{1 - \frac{\eta_{\parallel,\perp}}{8}\frac{\varepsilon_{\mathrm{sub}}-\varepsilon_{\mathrm{med}}}{\varepsilon_{\mathrm{sub}}+\varepsilon_{\mathrm{med}}}\left[1 - f(t)\right]\right\}$ with a thickness-dependent factor $f(t) = \frac{4\varepsilon_{\mathrm{sub}}\varepsilon_{\mathrm{med}}}{(\varepsilon_{\mathrm{sub}}+\varepsilon_{\mathrm{med}})^2}\left(\frac{1}{1+t/R}\right)^3$. Accordingly, the substrate-dependent redshift reduces with decreasing *t*; a feature which is supported by the results presented here.

Moreover, we observe an increased background signal with increasing *t*, most notable for particles supported on Si and SiN_x substrates. The appearance of a substrate related background signal in SiN_x is surprising, given that no losses are expected in this material below ~ 5 eV (see permittivity functions in Figures S1 and S2 in SI). We attribute this effect to Čerenkov losses, which occur when the speed of electrons exceeds the speed of light in a material [52,53]. The probability of Čerenkov radiation emission increases with the refractive index of a material and thickness (see Figures S3, S4 and S5 in SI). At the accelerating voltage employed in our experiments (120 kV) electrons travel at the speed 0.59*c*, where *c* is the speed of light, and Čerenkov losses are expected to be emitted in materials with refractive indices above ~ 1.7. The refractive index of SiN_x remains above this threshold value within the whole energy range studied and consequently, Čerenkov losses are present in our spectra. An even larger Čerenkov contribution is present for Si, which has a larger refractive index than SiN_x. Conversely, the refractive index of SiO_2 remains below the threshold value and minimal background signal is detected, even from thicker substrates.

NANOPARTICLE MATERIAL. Besides substrate related properties, the nanoparticle itself also has a striking influence on the extent of modifications introduced by the substrate: contrary to Ag nanoparticles, the plasmonic response of Au nanoparticles shows only a weak dependence on the presence or choice of a substrate. This anomalous difference in the behaviour of Au arises from the strong screening of plasmon excitations by its bound electrons[9,54,55] and can be understood by considering a simple non-retarded description of the LSP frequency of a nanosphere in a homogeneous embedding. For a metallic nanosphere with permittivity $\varepsilon(\omega) = \varepsilon_{\mathrm{B}}(\omega) - \omega_{\mathrm{P}}^2/\omega^2$ and fully embedded in a medium with permittivity $\varepsilon_{\mathrm{med}}$, the l^{th} order LSP frequency is given by[56]:

$$\omega_l = \frac{\omega_\mathrm{p}}{\sqrt{\varepsilon_\mathrm{B} + \frac{l+1}{l}\varepsilon_\mathrm{med}}} \quad (2)$$

where ω_p is the bulk plasmon frequency and ε_B is the contribution of the bound electrons to the permittivity of the metal, *i.e.* ε_B's deviation from unity accounts for effects beyond the free-electron, or Drude behavior (*e.g.* due to interband transitions). It is clear that in cases where $\varepsilon_\mathrm{B} >> \varepsilon_\mathrm{med}$, the LSP frequency shows only a weak dependence on changes in ε_med. This effect is further accentuated for particles supported on a substrate (in effect, being partially embedded). As a result, the large bound response of Au near the LSP frequencies (see Figure S6 in SI) masks the influence of the substrate dielectric properties, explaining the observed weak LSP dependence on substrate material for Au nanoparticles. In comparison, the bound response of Ag is significantly less pronounced than that of Au near the LSP resonance and accordingly, the substrate dependence is clearly discernible for Ag.

SUMMARY AND CONCLUSIONS

Our systematic investigation of the substrate effect on the EELS measurements of LSPs in nanoparticles confirms the considerable influence of both the substrate material and thickness. In particular, in the case of Ag nanoparticles, the presence of a dielectric substrate was shown to lead to redshift of the LSPs, higher probability of exciting HO modes and increasing line-widths of the plasmon features. The plasmonic response of Au nanoparticles were to a significantly smaller extent affected by the substrate choice, owing to the large contribution from the bound polarization in Au. More relevant to the EELS analysis of Au nanoparticles is the signal to noise ratio of the measurements, as the LSPs in Au are highly damped due to interband transitions. Substrate-related losses in the EELS signal exacerbated this issue by further reducing the visibility of the signal from the nanoparticles. Our results also demonstrate the paramount importance of the choice of electron beam impact parameter when probing distinct plasmonic modes is intended, as the EELS signal features most prominently the HO LSPs at small *b* and the dipolar LSP at large *b*. The threshold *b* for these two regions, however, is strongly dependent on substrate material and thickness.

Given that the typical set-up in EELS relies on a substrate to support the particles during the examination, a pertinent question is which substrate to choose. Our results demonstrate that the extent of substrate induced modifications generally increase with ε_sub and *t* and thus, if probing the plasmonic properties of nanostructures in vacuum is desired, substrates with large ε_sub and *t* should be avoided. Choosing substrates with large ε_sub and *t*

provide the opportunity to study, for example, HO LSPs[28] and energy transfer between the LSPs and the substrate[35]. However, it could be necessary to take Čerenkov radiations or other substrate related losses into consideration when analyzing the results. Finally, care must be taken in interpretation of EEL spectra with regards to the electron beam impact parameter: a pitfall lies in cases where dipolar and HO modes are excited with comparable probabilities (for example, when $b \sim R$ or when employing a substrate with large ε_{sub} and t) but cannot be resolved individually, due to insufficient energy resolution in EELS, resulting instead in the detection of a broad compounding peak, whose center energy does not necessarily correspond to any dipole or HO LSPs. Examining the evolution of the signal with beam impact parameter position is thus imperative in EELS analysis of plasmonic structures.

METHODS

Colloidal Ag and Au nanoparticles with respective diameters of 20 nm and 50 nm and approximately spherical geometries were studied here. Ag nanoparticles in an aqueous 2 mM citrate solution were purchased from nanoComposix, Inc. and an aqueous solution containing the Au nanoparticles were purchased from BBI Life Sciences. TEM specimens were prepared by depositing a drop of the solution containing the nanoparticles on a TEM grid and allowing the liquid to evaporate before examination with TEM. Three popular amorphous substrate materials (purchased from TEMwindows), spanning a range of optical material properties, were examined: silicon dioxide (SiO_2), silicon nitride (SiN_x), and silicon (Si). In each case the influence of the substrate thickness was also investigated by repeating the experiment for two different thicknesses. Scanning TEM (STEM) images and EELS measurements were carried out using an FEI TEM instrument fitted with a monochromator, probe aberration corrector and Gatan GIF Tridium 865 spectrometer. The TEM instrument was operated at an accelerating voltage of 120 kV, probe convergence angle of 25 mrad, EELS collection angle of 28 mrad and with a resulting imaging resolution of ~ 5 Å and energy resolution of ~ 0.15 eV. EELS spectra in the form of line scans across the particles were acquired with typical dwell time of ~ 100 ms. The EELS spectra were analyzed after deconvolution of the zero-loss peak (ZLP), using a power law function to fit the tail of the ZLP[57]. Resonance peak positions and full widths at half maximum were estimated by fitting features to a Gaussian model.

Theoretical simulations were computed by means of the retarded boundary element method[58], as implemented in the MNPBEM toolbox[59,60], which solves Maxwell's equations in the presence of a swift electron (accelerating

voltage of 120 keV) normally incident upon the nanoparticle-substrate plane. Both nanoparticle and substrate were discretized in triangular elements, and the substrate was treated as a finite radial disk with open lateral boundaries of sufficient radial extent to ensure convergence. Similarly, to ensure convergence the nanoparticles were artificially shifted 2 Å above the substrate. The dielectric properties of the constituent materials were taken from measured data, including spectral dispersion, specifically from Johnson and Christie[45] and Palik[61] for nanoparticle and substrate properties, respectively. For the purpose of comparison with the experimental data, the simulated EEL spectra were convolved with a Gaussian function with full width at half maximum equal to the energy resolution of the experiments (0.15 eV). The simulations performed for embedded nanoparticles do not include bulk and Čerenkov contributions from the embedding media.

ASSOCIATED CONTENT

Supporting Information containing additional figures accompanies this paper.

AUTHOR INFORMATION

Corresponding author:

* E-mail: shka@cen.dtu.dk

Notes:

The authors declare no competing financial interest.

ACKNOWLEDGMENTS

T.C. thanks Wei Yan for fruitful discussions. The A. P. Møller and Chastine Mc-Kinney Møller Foundation is gratefully acknowledged for their contribution towards the establishment of the Centre for Electron Nanoscopy at the Technical University of Denmark. T.C. acknowledges support from Villum Fonden.

REFERENCES

(1) Giannini, V.; Fernández-Domínguez, A. I.; Heck, S. C.; Maier, S. A. Plasmonic Nanoantennas: Fundamentals and Their Use in Controlling the Radiative Properties of Nanoemitters. *Chem. Rev.* **2011**, *111*, 3888–3912.

(2) Zia, R.; Schuller, J. A.; Chandran, A.; Brongersma, M. L. Plasmonics: The next Chip-Scale Technology. *Mater. Today* **2006**, *9*, 20–27.

(3) Linic, S.; Christopher, P.; Ingram, D. B. Plasmonic-Metal Nanostructures for Efficient Conversion of Solar to Chemical Energy. *Nat. Mater.* **2011**, *10*, 911–921.

(4) Anker, J. N.; Hall, W. P.; Lyandres, O.; Shah, N. C.; Zhao, J.; Van Duyne, R. P. Biosensing with Plasmonic Nanosensors. *Nat. Mater.* **2008**, *7*, 442–453.

(5) Jain, P. K.; El-Sayed, M. A. Surface Plasmon Coupling and Its Universal Size Scaling in Metal Nanostructures of Complex Geometry: Elongated Particle Pairs and Nanosphere Trimers. *J. Phys. Chem. C* **2008**, *112*, 4954–4960.

(6) Rossouw, D.; Couillard, M.; Vickery, J.; Kumacheva, E.; Botton, G. A. Multipolar Plasmonic Resonances in Silver Nanowire Antennas Imaged with a Subnanometer Electron Probe. *Nano Lett.* **2011**, *11*, 1499–1504.

(7) Sherry, L. J.; Chang, S.-H.; Schatz, G. C.; Duyne, R. P. Van; Wiley, B. J.; Xia, Y. Localized Surface Plasmon Resonance Spectroscopy of Single Silver Nanocubes. *Nano Lett.* **2005**, *5*, 2034–2038.

(8) Koh, A. L.; Bao, K.; Khan, I.; Smith, W. E.; Kothleitner, G.; Nordlander, P.; Maier, S. A.; McComb, D. W. Electron Energy-Loss Spectroscopy (EELS) of Surface Plasmons in Single Silver Nanoparticles and Dimers: Influence of Beam Damage and Mapping of Dark Modes. *ACS Nano* **2009**, *3*, 3015–3022.

(9) Lermé, J.; Bonnet, C.; Broyer, M.; Cottancin, E.; Manchon, D.; Pellarin, M. Optical Properties of a Particle above a Dielectric Interface: Cross Sections, Benchmark Calculations, and Analysis of the Intrinsic Substrate Effects. *J. Phys. Chem. C* **2013**, *117*, 6383–6398.

(10) Venkatapathi, M.; Kumar Tiwari, A. Radiative and Non-Radiative Effects of a Substrate on Localized Plasmon Resonance of Particles. *J. Appl. Phys.* **2012**, *112*, 13529.

(11) Swanglap, P.; Slaughter, L. S.; Chang, W. S.; Willingham, B.; Khanal, B. P.; Zubarev, E. R.; Link, S. Seeing Double: Coupling between Substrate Image Charges and Collective Plasmon Modes in Self-Assembled Nanoparticle Superstructures. *ACS Nano* **2011**, *5*, 4892–4901.

(12) Lermé, J. Plasmon Hybridization Model for a Nanoparticle above a Dielectric Interface: Dielectric Effects, Comparison with the Dimer System, Range of Applicability, and Limits. *J. Phys. Chem. C* **2015**, *119*, 21087–21104.

(13) Noguez, C. Surface Plasmons on Metal Nanoparticles: The Influence of Shape and Physical Environment.

J. Phys. Chem. C **2007**, *111*, 3806–3819.

(14) Yamagushi, T.; Yoshida, S.; Kinbara, A. Optical Effect of the Substrate on the Anomalous Absorption of Aggregated Silver Films. *Thin Solid Films* **1974**, *21*, 173–187.

(15) Jensen, T. R.; Duval, M. L.; Kelly, K. L.; Lazarides, A. A.; Schatz, G. C.; Van Duyne, R. P. Nanosphere Lithography: Effect of the External Dielectric Medium on the Surface Plasmon Resonance Spectrum of a Periodic Array of Silver Nanoparticles. *J. Phys. Chem. B* **1999**, *103*, 9846–9853.

(16) Malinsky, M. D.; Kelly, K. L.; Schatz, G. C.; Van Duyne, R. P. Nanosphere Lithography: Effect of Substrate on the Localized Surface Plasmon Resonance Spectrum of Silver Nanoparticles. *J. Phys. Chem. B* **2001**, *105*, 2343–2350.

(17) Félidj, N.; Aubard, J.; Lévi, G.; Krenn, J.; Schider, G.; Leitner, a.; Aussenegg, F. Enhanced Substrate-Induced Coupling in Two-Dimensional Gold Nanoparticle Arrays. *Phys. Rev. B* **2002**, *66*, 1–7.

(18) McMahon, J. M.; Wang, Y.; Sherry, L. J.; Duyne, R. P. Van; Marks, L. D.; Gray, S. K.; Schatz, G. C. Correlating the Structure, Optical Spectra, and Electrodynamics of Single Silver Nanocubes. *J. Phys. Chem. C* **2009**, *113*, 2731–2735.

(19) Ringe, E.; McMahon, J. M.; Sohn, K.; Cobley, C.; Xia, Y. N.; Huang, J. X.; Schatz, G. C.; Marks, L. D.; Van Duyne, R. P. Unraveling the Effects of Size, Composition, and Substrate on the Localized Surface Plasmon Resonance Frequencies of Gold and Silver Nanocubes: A Systematic Single-Particle Approach. *J. Phys. Chem. C* **2010**, *114*, 12511–12516.

(20) García de Abajo, F. J. Optical Excitations in Electron Microscopy. *Rev. Mod. Phys.* **2010**, *82*, 209–275.

(21) Colliex, C.; Kociak, M.; Stéphan, O. Electron Energy Loss Spectroscopy Imaging of Surface Plasmons at the Nanometer Scale. *Ultramicroscopy* **2015**, *162*, A1–A24.

(22) Iberi, V.; Mirsaleh-Kohan, N.; Camden, J. P. Understanding Plasmonic Properties in Metallic Nanostructures by Correlating Photonic and Electronic Excitations. *J. Phys. Chem. Lett.* **2013**, *4*, 1070–1078.

(23) Nelayah, J.; Kociak, M.; Stéphan, O.; García de Abajo, F. J.; Tencé, M.; Henrard, L.; Taverna, D.; Pastoriza-Santos, I.; Liz-Marzán, L. M.; Colliex, C. Mapping Surface Plasmons on a Single Metallic Nanoparticle. *Nat. Phys.* **2007**, *3*, 348–353.

(24) Nicoletti, O.; de la Peña, F.; Leary, R. K.; Holland, D. J.; Ducati, C.; Midgley, P. A. Three-Dimensional Imaging of Localized Surface Plasmon Resonances of Metal Nanoparticles. *Nature* **2013**, *502*, 80–84.

(25) Raza, S.; Stenger, N.; Pors, A.; Holmgaard, T.; Kadkhodazadeh, S.; Wagner, J. B.; Pedersen, K.; Wubs, M.; Bozhevolnyi, S. I.; Mortensen, N. A. Extremely Confined Gap Surface-Plasmon Modes Excited by Electrons. *Nat. Commun.* **2014**, *5*, 4125.

(26) Hobbs, R. G.; Manfrinato, V. R.; Yang, Y.; Goodman, S. A.; Zhang, L.; Stach, E. A.; Berggren, K. K. High-Energy Surface and Volume Plasmons in Nanopatterned Sub-10 Nm Aluminum Nanostructures. *Nano Lett.* **2016**, *16*, 4149–4157.

(27) Kadkhodazadeh, S.; de Lasson, J. R.; Beleggia, M.; Kneipp, H.; Wagner, J. B.; Kneipp, K. Scaling of the Surface Plasmon Resonance in Gold and Silver Dimers Probed by EELS. *J. Phys. Chem. C* **2014**, *118*, 5478–5485.

(28) Raza, S.; Kadkhodazadeh, S.; Christensen, T.; Di Vece, M.; Wubs, M.; Mortensen, N. A.; Stenger, N. Multipole Plasmons and Their Disappearance in Few-Nanometre Silver Nanoparticles. *Nat. Commun.* **2015**, *6*, 8788.

(29) Goris, B.; Guzzinati, G.; Fernández-López, C.; Pérez-Juste, J.; Liz-Marzán, L. M.; Trügler, A.; Hohenester, U.; Verbeeck, J.; Bals, S.; Van Tendeloo, G. Plasmon Mapping in Au@Ag Nanocube Assemblies. *J. Phys. Chem. C* **2014**, *118*, 15356–15362.

(30) Raza, S.; Stenger, N.; Kadkhodazadeh, S.; Fischer, S. V.; Kostesha, N.; Jauho, A. P.; Burrows, A.; Wubs, M.; Mortensen, N. A. Blueshift of the Surface Plasmon Resonance in Silver Nanoparticles Studied with EELS. *Nanophotonics* **2013**, *2*, 131–138.

(31) Guiton, B. S.; Iberi, V.; Li, S.; Leonard, D. N.; Parish, C. M.; Kotula, P. G.; Varela, M.; Schatz, G. C.; Pennycook, S. J.; Camden, J. P. Correlated Optical Measurements and Plasmon Mapping of Silver Nanorods. *Nano Lett.* **2011**, *11*, 3482–3488.

(32) Li, G.; Cherqui, C.; Wu, Y.; Bigelow, N. W.; Simmons, P. D.; Rack, P. D.; Masiello, D. J.; Camden, J. P. Examining Substrate-Induced Plasmon Mode Splitting and Localization in Truncated Silver Nanospheres with Electron Energy Loss Spectroscopy. *J. Phys. Chem. Lett.* **2015**, *6*, 2569–2576.

(33) Wu, Y.; Li, G.; Cherqui, C.; Bigelow, N. W.; Thakkar, N.; Masiello, D. J.; Camden, J. P.; Rack, P. D.

Electron Energy Loss Spectroscopy Study of the Full Plasmonic Spectrum of Self-Assembled Au − Ag Alloy Nanoparticles: Unraveling Size, Composition, and Substrate Effects. *ACS Photonics* **2016**, *3*, 130–138.

(34) Fujiyoshi, Y.; Nemoto, T.; Kurata, H. Substrate Effects on LSP of a Truncated Silver Nano-Sphere Observed by EELS. *Microscopy* **2015**, *64*, i99.

(35) Li, G.; Cherqui, C.; Bigelow, N. W.; Duscher, G.; Straney, P. J.; Millstone, J. E.; Masiello, D. J.; Camden, J. P. Spatially Mapping Energy Transfer from Single Plasmonic Particles to Semiconductor Substrates via STEM/EELS. *Nano Lett.* **2015**, *15*, 3465–3471.

(36) Christensen, T.; Yan, W.; Raza, S.; Jauho, A. P.; Mortensen, N. A.; Wubs, M. Nonlocal Response of Metallic Nanospheres Probed by Light, Electrons, and Atoms. *ACS Nano* **2014**, *8*, 1745–1758.

(37) Zhou, X.; Hörl, A.; Trögler, A.; Hohenester, U.; Norris, T. B.; Herzing, A. A. Effect of Multipole Excitations in Electron Energy-Loss Spectroscopy of Surface Plasmon Modes in Silver Nanowires. *J. Appl. Phys.* **2014**, *116*, 223101.

(38) Keast, V. J.; Walhout, C. J.; Pedersen, T.; Shahcheraghi, N.; Cortie, M. B.; Mitchell, D. R. G. Higher Order Plasmonic Modes Excited in Ag Triangular Nanoplates by an Electron Beam. *Plasmonics* **2016**, *11*, 1081–1086.

(39) Walter, J. P.; Cohen, M. L. Frequency- and Wave-Vector-Dependent Dielectric Function for Silicon. *Phys. Rev. B* **1972**, *5*, 3101–3110.

(40) Egerton, R. F. *Electron Energy-Loss Spectroscopy in the Electron Microscope*, 3rd ed.; Plenum Press: New York, 2011; pp 148.

(41) Kreibig, U.; Gonzel, L. Optical Absorption of Small Metallic Particles. *Surf. Sci.* **1985**, *156*, 678–700.

(42) Mortensen;, N. A.; Raza, S.; Wubs, M.; Søndergaard, T.; Bozhevolnyi, S. I. A Generalized Non-Local Optical Response Theory for Plasmonic Nanostructures. *Nat. Commun.* **2014**, *5*, 3809.

(43) v. Festenberg, C. Zur Dämpfung Des Al-15 eV-Plasmaverlustes in Abhängigkeit Vom Streuwinkel Und Der Kristallitgröße. *Zeitschrift Fur Phys.* **1967**, *55*, 47–55.

(44) Krishan, V.; Ritchie, R. H. Anomalous Damping of Volume Plasmons in Polycrystalline Metals. *Phys. Rev. Lett.* **1970**, *24*, 1117–1119.

(45) Johnson, P. B.; Christy, R. W. Optical Constants of the Noble Metals. *Phys. Status Solidi* **1972**, *1318*, 4370–4379.

(46) Wind, M. M.; Vlieger, J.; Bedeaux, D. The Polarizability of a Truncated Sphere on a Substrate I. *Physica A* **1987**, *141*, 33–57.

(47) Gozhenko, V.; Grechko, L.; Whites, K. Electrodynamics of Spatial Clusters of Spheres: Substrate Effects. *Phys. Rev. B* **2003**, *68*, 1–16.

(48) Quinten, M. *Optical Properties of Nanoparticle System*; Wiley-VCH: Weinheim, 2011; pp 199.

(49) Bohren, C. F.; Huffman, D. R. *Absorption and Scattering of Light by Small Particles*; Wiley-VCH, 1998; pp 147.

(50) Yan, W.; Mortensen, N. A.; Wubs, M. Green's Function Surface-Integral Method for Nonlocal Response of Plasmonic Nanowires in Arbitrary Dielectric Environments. *Phys. Rev. B* **2013**, *88*, 25–27.

(51) Egerton, R. F. Control of Radiation Damage in the TEM. *Ultramicroscopy* **2013**, *127*, 100–108.

(52) Stoger-Pollach, M.; Franco, H.; Schattschneider, P.; Lazar, S.; Schaffer, B.; Grogger, W.; Zandbergen, H. W. Cerenkov Losses: A Limit for Bandgap Determination and Kramers-Kronig Analysis. *Micron* **2006**, *37*, 396–402.

(53) Stoger-Pollach, M. Optical Properties and Bandgaps from Low Loss EELS: Pitfalls and Solutions. *Micron* **2008**, *39*, 1092–1110.

(54) Lazzari, R.; Jupille, J.; Cavallotti, R.; Simonsen, I. Model-Free Unraveling of Supported Nanoparticles Plasmon Resonance Modes. *J. Phys. Chem. C* **2014**, *118*, 7032–7048.

(55) Pakizeh, T. Optical Absorption of Plasmonic Nanoparticles in Presence of a Local Interband Transition. *J. Phys. Chem. C* **2011**, *115*, 21826–21831.

(56) Sernelius, B. E. *Surface Modes in Physics*; Wiley-VCH: Berlin, 2001; pp 261.

(57) Rafferty, B.; Pennycook, S. J.; Brown, L. M. Zero Loss Peak Deconvolution for Bandgap EEL Spectra. *J. Electron Microsc. (Tokyo).* **2000**, *49*, 517–524.

(58) García de Abajo, F. J.; Howie, A. Retarded Field Calculation of Electron Energy Loss in Inhomogeneous Dielectrics. *Phys. Rev. B* **2002**, *65*, 115418–17.

(59) Hohenester, U.; Trügler, A. MNPBEM - A Matlab Toolbox for the Simulation of Plasmonic

Nanoparticles. *Comput. Phys. Commun.* **2012**, *183*, 370–381.

(60) Hohenester, U. Simulating Electron Energy Loss Spectroscopy with the MNPBEM Toolbox. *Comput. Phys. Commun.* **2014**, *185*, 1177–1187.

(61) *Handbook of Optical Constants of Solids*; Palik, E. D., Ed.; Academic Press: San Diego, 1985.